Published in final edited form as:
Dev Dyn. 2009 January ; 238(1): 86–99. doi:10.1002/dvdy.21821.

Muscle degeneration and leukocyte infiltration caused by mutation of zebrafish Fad24

Kevin B. Walters[1,2], **M. Ernest Dodd**[2], **Jonathan R. Mathias**[2], **Andrea J. Gallagher**[2], **David A. Bennin**[2], **Jennifer Rhodes**[3], **John P. Kanki**[3], **A. Thomas Look**[3], **Yevgenya Grinblat**[4], and **Anna Huttenlocher**[1,2,*]

[1] Program in Cellular and Molecular Biology, University of Wisconsin-Madison; Madison, WI 53706; USA

[2] Department of Pediatrics and Medical Microbiology and Immunology; University of Wisconsin-Madison; Madison, WI 53706; USA

[3] Department of Pediatric Oncology; Dana-Farber Cancer Institute; Boston, MA 02115; USA

[4]Departments of Zoology and Anatomy, University of Wisconsin-Madison; Madison, WI 53706; USA

Summary

Factor for adipocyte differentiation 24 (fad24) is a novel gene that has been implicated in adipocyte differentiation and DNA replication. In a screen for zebrafish mutants that have an abnormal tissue distribution of neutrophils we identified an insertional allele of *fad24*, fad24^{hi1019}. Homozygous fad24^{hi1019} larvae exhibit muscle degeneration accompanied by leukocyte infiltration. Muscle degeneration was extensive and included tissue apoptosis and disorganized, poorly striated muscle fibers. Blocking apoptosis using pan-caspase inhibitors resulted in decreased neutrophil recruitment into the body of the larva, suggesting a causative link between apoptosis and leukocyte infiltration. These findings suggest that zebrafish is a powerful genetic model system to address the interplay between muscle degeneration and leukocyte infiltration, and indicate that tissue apoptosis may contribute to neutrophil recruitment in some inflammatory states.

Keywords

zebrafish; fad24; neutrophil; inflammation

Introduction

The zebrafish, *Danio rerio*, is an emerging model system for examining mechanisms of leukocyte recruitment and human disease. Zebrafish have an immune system that is highly homologous to that of humans, and are being used to study mechanisms of vertebrate hematopoiesis (Crowhurst et al., 2002; Onnebo et al., 2004; de Jong and Zon, 2005) and host-pathogen interactions (Davis et al., 2002; van der Sar et al., 2003; Miller and Neely, 2004). Recently, zebrafish models of acute inflammation have been described using transgenic zebrafish that allow for high-resolution observations of leukocyte recruitment as they respond to wounds or experimental infection (Mathias et al., 2006; Renshaw et al., 2006; Hall et al., 2007; Meijer et al., 2007). These reports demonstrate that acute inflammation in zebrafish involves the active recruitment of neutrophils into tissues followed by resolution by retrograde

*Corresponding author. Mailing address: 4205 Microbial Sciences Building, 1550 Linden Dr., Madison, WI 53706; Phone: (608) 259-9455; FAX: (608) 262-1257. huttenlocher@wisc.edu.

chemotaxis (Mathias et al., 2006) or apoptosis (Renshaw et al., 2006). In contrast, the first zebrafish model of chronic inflammation was recently described and was characterized by long-term retention of neutrophils in inflamed tissues in the absence of experimentally induced inflammatory stimuli or signs of inflammatory resolution (Mathias et al., 2007).

To identify genes involved in inflammation we screened a collection of zebrafish mutant lines for abnormal tissue distribution of neutrophils. This collection was generated by retrovirus insertional mutagenesis (Amsterdam et al., 1999) which allows rapid identification of mutated genes (Amsterdam et al., 2004). We have previously described a mutant line identified in this screen, *hi2217*, that showed leukocyte recruitment in areas of epidermal hyperproliferation in the fin due to an insertion in hepatocyte growth factor activator inhibitor 1 (*hai1*) (Mathias et al., 2007). Here we describe a second line identified in this screen, designated *hi1019* that carries an insertion in factor for adipocyte differentiation 24 (*fad24*, also known as *noc3l* and *ad24*). Fad24^{hi1019} homozygotes display a phenotype that has some characteristics of chronic inflammation, namely leukocyte infiltration into the trunk of developing larvae without signs of resolution.

Fad24 was originally identified in mammals during a screen looking for genes that are upregulated during the early stages of adipogenesis. Fad24 is an important regulator of adipocyte differentiation in cell culture and is expressed in a variety of human tissues. The protein contains a bZIP-like domain often found in transcription factors and a NOC domain found in proteins involved in rRNA processing and replication initiation (Tominaga et al., 2004). Further work exploring the function of Fad24 demonstrated that it is responsible for recruitment of HBO1, a histone acetyltransferase, to the origin of DNA replication and that together Fad24 and HBO1 are needed for the initiation of DNA replication that precedes adipocyte differentiation (Johmura et al., 2007). The role of *fad24* has not been explored in vivo during development, and no reports linked *fad24* to muscle degeneration or leukocyte recruitment to tissues.

Here we show that *fad24* function is required for the correct formation of several tissues, including muscle, during embryonic and larval development. Abnormal infiltration of leukocytes is observed in the body of fad24^{hi1019} larvae in areas of increased apoptosis and disorganized muscle fibers. We further show that neutrophil recruitment can be partially blocked by treating mutant larvae with pan-caspase inhibitors suggesting that apoptosis is at least partially responsible for the leukocyte recruitment. This study illustrates the utility of zebrafish as a model system to study factors that regulate neutrophil recruitment into tissues and to study the interplay between tissue damage and leukocyte recruitment.

Results

Expression of fad24 is disrupted by the hi1019 insertion

To identify genes involved in the regulation of inflammation, we performed a whole-mount in situ hybridization (WISH)-based screen on a collection of zebrafish insertional mutants (Amsterdam et al., 2004). Embryos at 2-3 days post fertilization (dpf) were stained for expression of the zebrafish neutrophil marker, myeloperoxidase (*mpo*). Of the 276 lines screened, 3 demonstrated an abnormal tissue distribution of neutrophils. One of these lines, *hi2217*, has been previously reported (Mathias et al., 2007), and here we discuss the characterization of a second line designated *hi1019*. By 3 dpf larvae homozygous for the *hi1019* insertion exhibited several developmental defects, including reduced overall body size, defective jaws and retinae, misshapen yolk sac, abnormal melanocyte distribution, and abnormal somites (Fig. 1A,A′, Fig. 7B,B′). Further analysis revealed that fad24^{hi1019} mutants fail to form musculature of the jaw (Fig. S1A,A′,B,B′), display misfolded hearts (Fig. S1C,C′) and have defects in gut formation (Fig. S1D,D′). These phenotypes first manifested at 3 dpf

while at younger stages mutants were morphologically indistinguishable from their wild-type (WT) siblings (data not shown). Furthermore, at 3 dpf neutrophils that normally reside in the head or caudal hematopoietic tissue (CHT) of WT larvae (Fig. 1B) infiltrated into the body of fad24^{hi1019} homozygotes (Fig. 1B′). In addition, the total number of neutrophils in the mutants was reduced by approximately 36% compared WT (Fig. 2F).

The *hi1019* insertion has previously been mapped to the first intron of the gene *fad24* (Fig. 1C) (Amsterdam et al., 2004). RT-PCR on total RNA isolated from single fad24^{hi1019} homozygotes or from WT larvae at 3 dpf using primers located in exon 1 and exon 2 of zebrafish *fad24* showed a decrease in *fad24* transcripts in mutants (Fig. 1D), demonstrating that the insertion significantly reduced *fad24* transcription or transcript stability. Amplification from contaminating genomic DNA would result in products about 2000 base pairs larger than amplification from cDNA, thus providing a means to distinguish the two. To address the possibility that fad24^{hi1019}mutants express a truncated transcript that would not be detected using the primer set described above, a second primer set was designed to amplify the region from exon 7 to exon 12 of *fad24*. A similar decrease in *fad24* transcripts was detected using this primer set (data not shown), suggesting that there is no truncated transcript present in fad24^{hi1019}mutants. In addition, a similar lack of transcript was detected in embryos from fad24^{hi1019} clutches at multiple developmental stages as early as 24 hpf (data not shown).

In humans, *fad24* is expressed in a variety of tissues, including muscle (Tominaga et al., 2004). We detected expression of *fad24* in the eye, brain and posterior somites at 26 hours post fertilization (hpf) by WISH (Fig. 1E). At 3 dpf expression of *fad24* was seen in the head, yolk and trunk of WT larvae, and *fad24* expression was significantly reduced in fad24^{hi1019} mutants (Fig. 1F,F′). The antisense *fad24* RNA probe used for this analysis is nearly full-length and should have detected any alternatively spliced transcripts, if they were present, in fad24^{hi1019} larvae. We conclude that the *hi1019* retroviral insertion causes a complete or near-complete loss of function of *fad24*.

Fad24 loss of function is responsible for the developmental defects and for abnormal leukocyte infiltration observed in hi1019 line

To confirm that *fad24* loss of function caused the *hi1019* phenotype, morpholino oligonucleotides (MOs) targeting *fad24* were injected into WT embryos. Two MOs were designed to target either the translational start site of *fad24* (zfad24 init), in order to block translation, or the splice junction between exon 17 and intron 17 (zfad24 ex17). Targeting of this splice junction should result in a complete or partial elimination of exon 17 which codes for the majority of the bZIP domain of Fad24, a domain required for the proper localization of human Fad24 in cell culture (Tominaga et al., 2004). Injection of either MO phenocopied the *hi1019* leukocyte redistribution phenotype as seen by Sudan Black staining to reveal neutrophil localization (Fig. 2 A-D). Quantification of neutrophil localization showed a clear increase in neutrophils recruited to the body of *fad24* MO injected larvae compared to both WT and control MO injected larvae (Fig. 2F). Each MO injected individually phenocopied the major morphological abnormalities observed in the fad24^{hi1019} mutants. In particular, jaws fail to form in both the translation-blocked and splice inhibited morphants, as they do in the mutants (Fig. 3A,C,E,G,I). Retinae are reduced to a similar extent in mutants and both morphants (Fig. 3A,C,E,G,I,K) and in the trunk, somite boundaries are poorly defined in the morphants as they are in the mutants (Fig. 3 B,D,F,H,J).

To confirm that the splicing MO affected splicing at the intended junction, RT-PCR was performed on total RNA isolated from uninjected controls, control MO-injected and zfad24 ex17 MO injected embryos using primers located in exon 16 and exon 18 of *fad24*. This analysis revealed that zfad24 ex17 MO injected embryos had reduced expression of correctly spliced *fad24* transcript compared to control embryos and showed expression of two misspliced

transcripts (Fig. 2E). Together, our findings strongly suggest that loss of fad24 function causes the major defects observed in fad24^{hi1019} homozygotes.

Zebrafish fad24 localizes to granules in the nucleus

Human Fad24 has been shown to localize to unidentified nuclear granules in transfected HeLa cells (Johmura et al., 2007). To determine the cellular localization of zebrafish Fad24 (zFad24) a fusion construct was made tagging EGFP to the N-terminus of zFad24. Transfection of this construct into HEK cells showed that full-length zFad24 also localized to the nucleus and was often found in distinct nuclear granules (Fig. 4B). To determine the subcellular localization of EGFP-zFad24 in zebrafish the fusion construct including the CMV promoter was subcloned into a Tol2 vector to allow for early genome integration and high levels of transient expression when coinjected with transposase mRNA at the one-cell stage (Kawakami et al., 2004). Transient expression of EGFP-zFad24 could be seen throughout the larva, most clearly in muscle fibers. Whereas EGFP was distributed throughout the muscle fiber cytoplasm (Fig. 4C), EGFP-zFad24 showed a punctate distribution, consistent with nuclear localization (Fig. 4D). Although ectopic zFad24 was produced, it did not rescue the mutant phenotype at 3 dpf. The lack of phenotypic rescue may be due to mosaicism inherent in the transient overexpression assay, or to a requirement that Fad24 be expressed at the proper levels in order to function correctly. Similarly we observed no phenotypic rescue when embryos were injected with in vitro transcribed zebrafish *fad24* mRNA. These results indicate that full-length zFad24 has a similar subcellular localization to human Fad24.

Zebrafish fad24 regulates lipid metabolism in vivo

Previous studies have reported that human Fad24 is a positive regulator of adipocyte differentiation in cell culture systems (Tominaga et al., 2004). To determine if zebrafish Fad24 has a similar function in vivo, larvae were stained for neutral fat using oil red O. Staining of WT larvae at 3 dpf revealed concentrated lipids in portions of the head, eye, and heart (Fig. 5A arrows), consistent with previous reports (Schlombs et al., 2003). In addition, lipids could be seen associated with the vasculature (Schlegel and Stainier, 2006) (Fig. 5A arrowheads). In fad24^{hi1019} mutants, reduced lipid concentrations were observed in all of these areas (Fig. 5A ′) yet the yolk sac of both WT and mutant larvae stained heavily with oil red O (Fig. 5A,A′). Injection of the zfad24 init. MO also resulted in loss of oil red O staining (Fig. 5B,C). Together, these results suggest an important role for zFad24 in lipid metabolism during zebrafish development.

Neutrophils and macrophages infiltrate the trunk of fad24^{hi1019} mutants

To characterize the leukocyte redistribution phenotype in fad24^{hi1019} mutants, neutrophil localization was examined at different developmental stages. In general, neutrophil distribution was normal until 2.5 dpf (data not shown), and by 3 dpf, all mutants showed extensive infiltration of neutrophils into the trunk (Fig. 6A,A′). L-plastin, a marker for macrophages in early embryos (Herbomel et al., 1999; Bennett et al., 2001; Su et al., 2007) and leukocytes in older embryos (Meijer et al., 2007) showed a similar abnormal distribution in fad24^{hi1019} mutants (Fig. 6B,B′). Overlay to examine both MPO and L-plastin staining revealed that all MPO^{+} cells (neutrophils) also expressed L-plastin. However a subpopulation of L-plastin^{+} cells did not express MPO (Fig. 6C,C′). Closer examination of the MPO^{-} L-plastin^{+} population showed that they had a more elongated morphology than neutrophils (Fig. 6D) and likely represented macrophages. To confirm that macrophages are involved in the inflammatory response in fad24^{hi1019} mutants, we examined expression of *c-fms* (*csf1r*), a separate macrophage marker that does not co-express with *mpo* (Meijer et al., 2007; Su et al., 2007). In WT siblings the majority of *c-fms*$^{+}$ leukocytes were found in the CHT (Fig. 6E) while in fad24^{hi1019} homozygotes *c-fms*$^{+}$ leukocytes had infiltrated into the body (Fig. 6E′). Together,

these findings suggest that both neutrophils and macrophages infiltrate into the trunk of fad24^{hi1019} larvae.

To better determine the tissue localization of neutrophils in fad24^{hi1019} mutants optical sectioning using a confocal microscope was done on MPO immunolabeled larvae. Projections in the Z direction show that neutrophils infiltrated into much deeper tissues in mutants compared to WT larvae (Fig. 6F,F′). Co-immunolabeling with an antibody to p63, a marker of epidermal cells, demonstrated limited inflammation in the epidermis with most neutrophils being found in deeper tissues (Fig. 6G,G′) including muscle (Fig. 6H). Together this suggests that neutrophils are recruited to multiple tissues in fad24^{hi1019} mutants and recruitment is not limited to the epidermis as described for the previously published *hi2217* inflammation mutant (Mathias et al., 2007).

To determine the subcellular localization of MPO and L-plastin in neutrophils from fad24^{hi1019} larvae we used high magnification confocal microscopy on immunolabeled larvae. Localization of L-plastin is peripheral with concentration at the membrane while MPO is localized to distinct cytoplasmic granules (Fig S2D,E) similar to what has been observed in neutrophils at a wound in WT embryos (data not shown). This suggests that neutrophils in fad24^{hi1019} larvae have a normal complement of MPO containing granules in the cytoplasm. Furthermore, MPO in the mutants appears to be active when examined by whole mount endogenous MPO activity assay (Fig. S2F,F′).

To generate a model to visualize the leukocyte trafficking in real-time, fad24^{hi1019} carriers were crossed to Tg(*mpx:GFP*)uwm1 transgenic fish, in which neutrophils express GFP (Mathias et al., 2006). Time-lapse confocal imaging of fad24^{hi1019};*mpx:GFP* larvae at 3 dpf revealed extensive infiltration of highly motile neutrophils into the trunk (see Movie 1 in supplementary material). In contrast, neutrophils in WT larvae were less migratory and remained primarily in the CHT and in the yolk extension, with the exception of one neutrophil that migrated through the body at the level of the horizontal myoseptum (see Movie 2 in supplementary material). Neutrophil migration in *fad24* mutants appeared similar to that reported in the tailfin of *hai1* mutants (Mathias et al., 2007). Neutrophils did not accumulate in specific areas and did not show reverse migration to the vasculature or CHT as observed in wounded WT embryos (Mathias et al., 2006). Wounding the fin of fad24^{hi1019} larvae resulted in neutrophil recruitment, suggesting that neutrophil recruitment to acute inflammatory stimuli is not impaired in the *fad24* mutants (Fig. S2 A, see Movie 3 and 4 in supplementary material). A subpopulation of cells expressing low levels of MPO has been described in the Tg (*mpx:GFP*)uwm1 transgenic line (Mathias et al., 2006) and it was suggested that these cells may be macrophages. This cell population can be distinguished in *fad24^{hi1019};mpx:GFP* larvae (Fig. S2C) and can be found migrating randomly through the body of larvae (see Movie 3 in supplementary material) and responding to wounds inflicted in the fin (Fig. S2 B,C, see Movie 3 and 4 in supplementary material). Taken together, we were not able to detect any defects in migration, morphology or function of neutrophils or macrophages from fad24^{hi1019} larvae compared to their WT siblings.

Fad24^{hi1019} mutants display decreased muscle organization

Tissue infiltration by neutrophils in fad24^{hi1019} mutants is primarily restricted to the trunk, where *fad24* is expressed at 3 dpf (Fig. 1F) and obvious body patterning defects can be seen (Fig. 1 A,A′). To determine if defects in muscle architecture exist in *fad24* mutants, polarized light microscopy was used to view the birefringence of trunk muscle. Birefringence was reduced in the skeletal muscle of the trunk of fad24^{hi1019} mutants compared to WT (Fig. 7A,A′), similar to what has been reported for zebrafish with mutations in structural muscle genes (Granato et al., 1996;Behra et al., 2002;Etard et al., 2005). In addition, mutants showed reduced definition of somites in the trunk (Fig. 7B,B′). To examine muscle fiber organization, muscle

fibers were immunolabeled using antibodies specific for fast-muscle or slow-muscle myosin. Confocal images of immunolabeled larvae stained with EB165, a fast-muscle myosin-specific antibody, revealed a general disorganization of muscle fiber clusters in the mutants (Fig. 7C,C′) Mutant muscle fibers were smaller in width compared to WT and had significantly fewer striations (Fig. 7Ca,C′a). Staining with F59, a slow-muscle myosin-specific antibody, revealed a similar disorganization of the slow muscle fibers in fad24^{hi1019} mutants (Fig. 7D,D′). Hematoxylin and eosin stained longitudinal sections taken through the developing somites of 3 dpf larvae also clearly showed differences in muscle fiber size and striation (Fig. 7E,E′). To examine somite structure we stained larvae for expression of a myoseptum marker cb1045 (Thisse et al., 2004;Deniziak et al., 2006). Fad24^{hi1019} mutants showed normal myoseptum (Fig. 7F,F′) demonstrating that somite boundaries were intact in the mutants. The touch-provoked swim response of mutant larvae was also defective at 3 dpf, and mutant fish tended to swim in circles with poorly coordinated tail movements (data not shown). The larvae displayed progressive muscle degeneration and were generally unable to swim at 5 dpf (data not shown). Taken together, the findings suggest that the fad24^{hi1019} mutants display leukocyte infiltration into areas of progressive muscle degeneration.

Leukocytes are not required for the onset of muscle degeneration

Human muscle diseases are often associated with leukocyte infiltration and in some cases this can contribute to the progression of disease (Formigli et al., 1992; Hodgetts et al., 2006). To determine if the leukocyte infiltration observed in fad24^{hi1019} mutants is responsible for the onset of the muscle degeneration, *pu.1* (also known as *spi1*), a transcription factor required for neutrophil and macrophage development in zebrafish, was knocked down using a previously characterized MO (Rhodes et al., 2005; Su et al., 2007). Injection of the *pu.1* MO successfully reduced neutrophil numbers in WT and mutant larvae at 3 dpf (Fig. 8C,D), but did not alleviate the early (3 dpf) muscle degeneration phenotype (Fig. 8B,D,Ba,Da). These results indicate that neutrophils and macrophages do not cause the initial muscle defect in fad24^{hi1019} mutants. However, since the MO was not effective at eliminating leukocytes after 3 dpf, we were not able to determine if leukocytes play a role in the progression of muscle degeneration in the fad24^{hi1019} mutant larvae (data not shown).

Apoptosis in the muscle of fad24^{hi1019} contributes to the recruitment of neutrophils

To determine if fad24^{hi1019} mutants display apoptosis in areas of abnormal leukocyte recruitment and muscle degeneration TUNEL and acridine orange staining were performed. TUNEL labeling revealed an increase in apoptosis in the body of fad24^{hi1019} mutants compared to WT larvae (Fig. 9A,A′) that did not overlap with MPO immunolabeling (Fig. 9B), consistent with apoptosis in tissues of the trunk. Staining live larvae with acridine orange also showed increased apoptosis in the mutants (Fig. 9C,C′). Interestingly, delivery of the pan-caspase inhibitors zVD.fmk or Q-VD-OPh to fad24^{hi1019} larvae resulted in an elimination of acridine orange staining in the body of mutant larvae (Fig. 9D,D′ and data not shown). Treatment with caspase inhibitors also reduced neutrophil infiltration into the body of the zebrafish by 50% (Fig. 9E,E′,F), suggesting that tissue apoptosis is an important factor involved in recruiting neutrophils into the trunk of the fad24^{hi1019} mutant larvae. Taken together these findings suggest that neutrophilic infiltration is mediated in part by tissue apoptosis in fad24^{hi1019} mutants.

Discussion

In this report we identify *fad24* as a novel regulator of muscle integrity and leukocyte recruitment in vivo. This identification is based on muscle degeneration and abnormal leukocyte infiltration observed in fad24^{hi1019} mutants. The abnormal leukocyte distribution and muscle degeneration were accompanied by increases in apoptosis in the trunk and we show

that inhibitors of caspase activity impair neutrophil recruitment in the *fad24* mutant. Taken together, these findings suggest that zebrafish is a powerful genetic model system to study the links between leukocyte recruitment, muscle degeneration and apoptosis in vivo.

This is, to our knowledge, the first paper to characterize in vivo functions for the regulator of adipogenesis, *fad24*. Previous studies have identified genes required for lipid metabolism (Schlombs et al., 2003; Schlegel and Stainier, 2006) or for skeletal muscle formation (Granato et al., 1996; Behra et al., 2002; Etard et al., 2005; Cheng et al., 2006; Deniziak et al., 2006; Seeley et al., 2007; Steffen et al., 2007). We identify *fad24* as a critical regulator of both lipid metabolism and muscle integrity and show that zebrafish Fad24 protein localizes to the nucleus and targets to nuclear granules, similar to the distribution of human Fad24 (Tominaga et al., 2004). Together, our findings suggest functional conservation between zebrafish and human *fad24*.

Fad24 mutants share phenotypic characteristics with zebrafish embryos that display embryonic malabsorption syndrome (EMS). For example, previous studies report that treatment of zebrafish embryos with clofibrate induces phenotypes characterized by unutilized yolk reserves, small eyes and head, jaw malformations, heart folding defects, and disorganized muscle fibers (Raldua et al., 2008), similar to what we observe with the *Fad24* mutants. Furthermore, the oil red O staining pattern observed in fad24^{hi1019} mutants is consistent with a failure of endogenous lipids found in the yolk to be properly transported to the rest of the larva, and is very similar to that described for clofibrate-treated embryos (Raldua et al., 2008) and with embryos deficient in the lipid transport protein *mtp* (Schlegel and Stainier, 2006). These findings support a role for zebrafish *fad24* in regulating embryonic lipid metabolism and suggest that some of the phenotypes observed in fad24^{hi1019} mutant larvae may be due to nutritional deprivation. Regulation of proper embryonic lipid metabolism is one potential mechanism through which *fad24* may indirectly regulate muscle integrity and leukocyte infiltration.

Previous studies have demonstrated high expression of human *fad24* in muscle tissue, however a functional role for *fad24* in human muscle has not been previously reported. *Fad24* expression is upregulated during myogenesis, suggesting that *fad24* may have an important role in regulating muscle development (Tominaga et al., 2004). We also find that zebrafish *fad24* is expressed in muscle (Fig. 1E). The muscle degeneration in the fad24^{hi1019} mutant is associated with a progressive defect in motor function, with the majority of mutants unable to swim after 5 dpf (data not shown). Our findings suggest that *fad24* is necessary for proper muscle development and integrity since *fad24*-deficient larvae display progressive muscle degeneration.

The *fad24* mutants had substantial leukocyte infiltration associated with the muscle degeneration. We and others have previously reported leukocyte infiltration associated with epithelial hyperproliferation (Carney et al., 2007; Mathias et al., 2007), but this is the first report of a mutant with leukocyte infiltration into other tissues. There have been previous reports of neutrophils associated with stressed tissues in other mutants (Le Guyader et al., 2008), however, we did not find abnormal neutrophil distribution to be a common feature of embryos with developmental defects, since only 3 out of 276 mutant lines we screened (fewer than 2%) showed leukocyte infiltration into tissues.

The signals that recruit neutrophils to damaged tissues remain largely unknown. A recent study reports that leukocyte infiltration into tissues can be associated with apoptotic clusters of keratinocytes in *hai1* deficient embryos, however no direct link between apoptosis and leukocyte recruitment was established (Carney et al., 2007). We find that fad24^{hi1019} larvae have increased numbers of apoptotic cells in areas where neutrophils are also observed.

Furthermore we show that inhibition of apoptosis with two different caspase inhibitors impairs neutrophil recruitment to the trunk of fad24^{hi1019} mutants. These findings suggest that apoptosis in tissues may be a significant factor that contributes to the neutrophil recruitment in the fad24^{hi1019} mutant. Alternatively, the reduced neutrophil recruitment into the body could be explained by the role some caspases play in the processing of proinflammatory cytokines (Thornberry et al., 1992; Martinon and Tschopp, 2007). We cannot, however, rule out the possibility that caspase inhibitors may have an off target effect on neutrophil development or motility. It is also important to note that the exact nature of the cell death seen by increased TUNEL and acridine orange staining is not known. TUNEL labels DNA fragmentation most often associated with apoptotic cells (Gavrieli et al., 1992) and the use of acridine orange to label apoptotic cells in zebrafish is well established (Parng et al., 2002; Tucker and Lardelli, 2007). Pan-caspase inhibitors block acridine orange staining suggesting apoptosis is involved, but we cannot rule out the possibility that some form of secondary necrosis is occurring in the body of the fad24^{hi1019} larvae.

It is also possible that *fad24* has a more direct role in regulating the inflammatory response. A recent report suggests that Fad24 regulates NF-κB activity by interacting with the p65 subunit (Johmura et al., 2008), providing an alternative mechanism by which Fad24 may regulate apoptosis and leukocyte recruitment. It is also possible that *fad24* affects inflammatory responses indirectly by regulating adipogenesis, since adipose tissue is a critical regulator of the inflammatory response through the release of inflammatory cytokines (Wisse, 2004). The exact nature of the cues responsible for mediating leukocyte recruitment in the fad24^{hi1019} mutants remain unknown, but likely involves a complex interplay between multiple factors.

Substantial evidence supports the validity of using zebrafish for modeling the pathogenesis of human muscular degenerative disorders. This evidence is derived from mutational analyses of structural genes such as titin (Xu et al., 2002; Steffen et al., 2007) and dystrophin (Guyon et al., 2003). Other important muscle structural proteins have been identified and characterized in zebrafish, including the key members of the dystrophin associated protein complex (Chambers et al., 2001; Parsons et al., 2002; Guyon et al., 2003). This report adds *fad24* to the list of genes with muscle degeneration phenotypes when mutated. Although leukocyte recruitment in fad24^{hi1019} mutants is not limited to muscle tissue, our findings suggest that zebrafish could provide a powerful model system to study the interplay between recruitment and muscle degeneration in zebrafish models of myopathies. Preliminary results from our laboratory indicate that neutrophilic infiltration is found in both dystrophin and titin-deficient zebrafish morphants or mutants (data not shown). There is substantial evidence to suggest that inflammation is involved in the clinical progression of muscular dystrophies (Grounds and Torrisi, 2004; Hodgetts et al., 2006; Whitehead et al., 2006). We find that leukoctye infiltration is not necessary for the onset of muscle defects in the fad24^{hi1019} mutants, however, we were not able to determine if leukocytes are involved in the progression of muscle degeneration because pu.1 MO knock-down was transient and leukocyte numbers recovered after 3 dpf. Future studies will be needed to determine the contribution of leukocytes to the progression of muscle degeneration in zebrafish models of myopathy.

Few studies have addressed the factors that regulate the recruitment of leukocytes to damaged or degenerative tissues. Our findings indicate that tissue apoptosis may contribute to leukocyte recruitment in the *Fad24* mutants and that inhibition of caspases may represent an attractive target to limit these responses. Furthermore, zebrafish models of leukocyte recruitment to tissues will provide powerful tools to screen for factors that regulate cell recruitment, and the fad24^{hi1019};*mpx:GFP* transgenic line can be used in large-scale chemical screens aimed at identifying novel compounds that target apoptosis or leukocyte recruitment.

Experimental Procedures

Zebrafish maintenance

All protocols using zebrafish in this study were approved by the University of Wisconsin-Madison Research Animal Resources Center. Adult zebrafish and embryos were maintained according to standard protocols (Nusslein-Volhard, 2002) and staged as previously described (Kimmel et al., 1995). Heterozygous *hi1019* (fad24^{hi1019},official designation noc3l^{hi1019}/noc3l^{+}) were crossed to Tg(*mpx:GFP*)uwm1 (Mathias et al., 2006) transgenic adults and raised; embryos from these crosses are referred to in this manuscript as fad24^{hi1019};*mpx:GFP*.

Image acquisition

Images were captured with either (1) a Nikon SMZ-1500 zoom microscope equipped with epifluorescent illumination, (2) a Nikon Eclipse TE300 inverted microscope equipped with epifluorescent illumination or (3) a Fluoview FV1000 FV10-ASW confocal laser scanning microscope. Color images were captured with NIS Elements D 2.30 software, confocal images were captured with Fluoview FV10-ASW software version 01.07, and all other images were captured and analyzed with MetaMorph software. The birefringence of the axial skeletal muscle was examined under polarized light on a Nikon SMZ-1500 zoom microscope as described previously (Felsenfeld et al., 1990).

Whole-mount in situ hybridization

The Hopkins mutant zebrafish collection (Amsterdam et al., 2004) was screened for expression of *mpo* by in situ hybridization. Briefly, embryos were obtained from crosses of adults known to be heterozygous for individual insertions, raised and fixed at 2-3 dpf in 4% paraformaldehyde in PBS; *mpo* mRNA was labeled by in situ hybridization as described previously (Bennett et al., 2001). Zebrafish *fad24* mRNA expression and the myoseptum was detected in 3 dpf larvae by the same protocol using probe cb522 (accession # CA408054) and probe cb1045 (accession # CF943681) respectively, as done previously (Thisse, 2001). The *c-fms* probe (Parichy et al., 2000; Herbomel et al., 2001) was kindly provided by L. Ramakrishnan.

Sudan Black staining

Neutrophils were detected using Sudan Black as previously reported (Le Guyader et al., 2008). After staining, larvae were incubated with a 1% KOH and 1% H_2O_2 solution at room temperature for 15 minuets to clear pigment from the larvae making it easier to visualize individual neutrophils.

Endogenous MPO activity assay

Larvae were fixed in 4% paraformaldehyde/PBS for 2 hours at room temperature. To detect MPO activity, a Sigma kit (390-A) was used as follows: Larvae were washed in 1× Trizmal (pH 6.3) containing 0.01% Tween-20 (TT) and then incubated at 37°C in TT containing 1.5 mg/ml substrate (supplied) and .015% hydrogen peroxide for 5-15 min. Larvae were then washed in PBS.

Oil red O staining

Larvae were stained with oil red O as described (Schlegel and Stainier, 2006). Briefly, larvae were fixed in 3.7% formaldehyde for 6 hours at 4°C, washed in PBS, and stained with filtered .3% oil red o (Sigma) in 60% 2-propanol for 2-3 hours at room temperature. Larvae were removed from stain and washed with PBS before imaging.

Zebrafish embryo sectioning

Larvae were fixed in 4% paraformaldehyde, washed in PBS, suffused in 30% sucrose and infiltrated with paraffin. Paraffin sections, 5 μm thick, were processed and stained with Hematoxylin and Eosin as described previously (Hsu et al., 2004).

RNA isolation and RT-PCR

Total RNA was isolated from single embryos or larvae using a STAT-60 (Tel-test, inc.) RNA isolation protocol. Briefly, 100 μl of STAT-60 was added to an embryo followed by vortexing. Debris was pelleted and the supernatant was extracted with chloroform. RNA was precipitated from the aqueous layer with isopropanol, washed, dried and resuspended in nuclease-free water. Zebrafish mRNA transcripts were detected by RT-PCR using a one-step kit purchased from Qiagen. Zebrafish *fad24* was detected using primer sets (5′-3′) CGGCAGTTTAAGCAACAGAGT and TCCTCCTGCTGCATCTTTCTG, TGCCGTCACCGTCAGAAAGTTAGT and TAGCTTCAGCTTCCAGCAGTTCCT, and to detect changes in *fad24* transcript due to zfad24 ex 17 splicing MO the primer set CCCTGAAATTCTACAGCCACTTG and GCGTCTCATTATCCAGAAGGATG was used.

Whole-mount immunolabeling

Zebrafish larvae were fixed in 4% paraformaldehyde in PBS overnight at 4°C, 1% formaldehyde in PBS for 2 hours at room temperature, or graded methanol in PBS at room temperature and immunolabeled as described previously (Mathias et al., 2006). Zebrafish MPO and L-plastin were detected using polyclonal antibodies (Mathias et al., 2006; Clay et al., 2007). Slow and fast muscle myosin were detected using monoclonal antibodies F59 and EB165, respectively and monoclonal antibody p63 (Novus Biological) was used at 1:250 to detect epidermal cells. F59, EB165, and A41025 were purchased from the developmental studies hybridoma bank and were used at 1:20. For MPO/L-plastin double-immunolabeling, larvae were fixed in 1% Formaldehyde/PBS for 2 hours at room temperature then labeled (as above) sequentially as follows: (1) rabbit anti-zMPO, (2) FITC-conjugated goat anti-rabbit Fab fragment (Jackson), (3) rabbit anti-L-Plastin IgG conjugated to Rhodamine Red using the FluoReporter Rhodamine Red-X Protein Labeling Kit (Molecular Probes), according to manufacturer's instructions.

TUNEL and Acridine Orange labeling

Apoptotic cells were fluorescently labeled by terminal deoxynucleotidyl transferase dUTP nick-end labeling (TUNEL) as described (Mathias et al., 2007). Apoptotic cells were also labeled by incubation of live zebrafish with 16.7 μg/ml acridine orange in E3 in the dark for 30 minutes. Larvae were washed with E3 and analyzed under a fluorescence microscope (Barrallo-Gimeno et al., 2004).

Morpholino oligonucleotide microinjection

Morpholino oligonucleotides (MO) were purchased from GeneTools, LLC (Philomath, OR, USA) and prepared as described (Mathias et al., 2007); Standard control MO sequence is available from GeneTools and was injected at the same (or greater) volume and concentration. pu.1 MO (1 nl at 1 mM injected) was used as described previously (Langheinrich et al., 2002; Rhodes et al., 2005). Other MO were designed to block translation or splicing of *fad24* transcripts (accession # NM_001002863).

zfad24 init (initiation site MO) 1 mM, 1 nl: GCCCATTTTGAGCGATGATTTGACT

zfad24 ex17 (splicing MO) 200 μM,1 nl : AGCAATGTCTCATCTCACCTGCATC.

zVD.fmk and Q-VD-OPh drug treatment

Larvae obtained from crosses of adults known to be heterozygous for the *hi1019* insertion were incubated in 100 μM zVD.fmk (Z-Val-DL-Asp-fluoromethylketone, Bachem), 50 μM Q-VD-OPh (Quinolyl-Val-Asp-OPh, R&D systems) or equal volume of DMSO in E3 at 28°C from 24 hpf to 3 dpf. Mutant larvae were then separated from WT and acridine orange or MPO antibody staining was performed as above. Three replicate experiments were done with an average sample size of 13 mutant larvae per condition for each experiment. Due to differences in neutrophil number from clutch to clutch, results are displayed as being relative to the DMSO control condition in each experiment. Average neutrophil counts from each experiment were analyzed by a paired student's t-test at a 95% confidence level. Due to differences in neutrophil number from clutch to clutch the average of each DMSO group was paired to the average of each zVD.fmk group for this analysis.

Cloning, cell culture, and transient expression in zebrafish

Fad24 was cloned using primers based on the Pubmed sequence, NM_001002863. RNA was isolated from 19 somite-staged embryos as above, and mRNA was enriched using Oligotex (Qiagen). SuperScript III One-Step RT-PCR System with Platinum Taq High Fidelity (Invitrogen) was used to amplify *fad24* which was subsequently cloned into pCR2.1 (Invitrogen). An EGFP tagged Fad24 was created for cell culture experiments by PCR amplification of the *fad24* sequence and cloning into pEGFP-C1 (Clontech). For transient overexpression of these constructs in zebrafish the entire EGFP-zFad24 cassette (including the CMV promoter) was cloned into a Tol2 vector. A construct containing full-length Tol2 transposon arms was kindly provided by Mike Nonet (Washington University, St. Louis) and was used to create a construct with minimal Tol2 elements for efficient integration, as described previously (Urasaki et al., 2006). Widespread expression of Tol2 EGFP-zFad24 or Tol2 EGFP was obtained by injection of 525 pl of 25 ng/μl plasmid with 35 ng/μl in vitro transcribed (Invitrogen) Tol2 transposase mRNA.

HEK293 fibroblasts were cultured in Dulbecco's modification of Eagles's Medium (Cellgro), containing 4.5g/L glucose, L-glutamine and sodium pyruvate supplemented with 100 U/ml penicillin, 100 μg/ml streptomycin (Cellgro) and 10% heat-inactivated fetal bovine serum (HyClone). Cells were transfected using 1μg DNA and 3μl Lipofectamine 2000 (Invitrogen) according to the manufacturer's instructions. At 24 hours post transfection cells were plated onto a glass coverslip coated with human fibronectin for 24 hours. Cells were then fixed with 3% formaldehyde, quenched in glycine and stained 30 minutes with DAPI (Molecular Probes).

Supplementary Material

Refer to Web version on PubMed Central for supplementary material.

Acknowledgments

We thank Adam Amsterdam and Nancy Hopkins (M.I.T.) for providing *hi1019* embryos, and Satoshi Kinoshita for histology. The monoclonal antibodies F59, EB165 and A4.1025 developed by Frank E. Stockdale, Everett Bandman and H.M. Blau respectively were obtained from the developmental studies hybridoma bank, Department of Biological Sciences, Iowa City, IA 52242. This work was supported by NIH grants to A.H. (R01 GM074827), J.R. (5KO1DK69672) and C.B. Thisse (RR15402-01, for cb522 and cb1045 EST) and the Hematology training grant (MED) and Arthritis Foundation (J.R.M.). The authors declare no conflicts of interest related to this work.

Grants: NIH: R01 GM074827, NIH: 5KO1DK69672, NIH: RR15402-01

References

Amsterdam A, Burgess S, Golling G, Chen W, Sun Z, Townsend K, Farrington S, Haldi M, Hopkins N. A large-scale insertional mutagenesis screen in zebrafish. Genes Dev 1999;13:2713–2724. [PubMed: 10541557]

Amsterdam A, Nissen RM, Sun Z, Swindell EC, Farrington S, Hopkins N. Identification of 315 genes essential for early zebrafish development. Proc Natl Acad Sci U S A 2004;101:12792–12797. [PubMed: 15256591]

Barrallo-Gimeno A, Holzschuh J, Driever W, Knapik EW. Neural crest survival and differentiation in zebrafish depends on mont blanc/tfap2a gene function. Development 2004;131:1463–1477. [PubMed: 14985255]

Behra M, Cousin X, Bertrand C, Vonesch JL, Biellmann D, Chatonnet A, Strahle U. Acetylcholinesterase is required for neuronal and muscular development in the zebrafish embryo. Nat Neurosci 2002;5:111–118. [PubMed: 11753420]

Bennett CM, Kanki JP, Rhodes J, Liu TX, Paw BH, Kieran MW, Langenau DM, Delahaye-Brown A, Zon LI, Fleming MD, Look AT. Myelopoiesis in the zebrafish, Danio rerio. Blood 2001;98:643–651. [PubMed: 11468162]

Carney TJ, von der Hardt S, Sonntag C, Amsterdam A, Topczewski J, Hopkins N, Hammerschmidt M. Inactivation of serine protease Matriptase1a by its inhibitor Hai1 is required for epithelial integrity of the zebrafish epidermis. Development 2007;134:3461–3471. [PubMed: 17728346]

Chambers SP, Dodd A, Overall R, Sirey T, Lam LT, Morris GE, Love DR. Dystrophin in adult zebrafish muscle. Biochem Biophys Res Commun 2001;286:478–483. [PubMed: 11511083]

Cheng L, Guo XF, Yang XY, Chong M, Cheng J, Li G, Gui YH, Lu DR. Delta-sarcoglycan is necessary for early heart and muscle development in zebrafish. Biochem Biophys Res Commun 2006;344:1290–1299. [PubMed: 16650823]

Clay H, Davis JM, Beery D, Huttenlocher A, Lyons SE, Ramakrishnan L. Dichotomous role of the macrophage in early Mycobacterium marinum infection of the zebrafish. Cell Host Microbe 2007;2:29–39. [PubMed: 18005715]

Crowhurst MO, Layton JE, Lieschke GJ. Developmental biology of zebrafish myeloid cells. Int J Dev Biol 2002;46:483–492. [PubMed: 12141435]

Davis JM, Clay H, Lewis JL, Ghori N, Herbomel P, Ramakrishnan L. Real-time visualization of mycobacterium-macrophage interactions leading to initiation of granuloma formation in zebrafish embryos. Immunity 2002;17:693–702. [PubMed: 12479816]

de Jong JL, Zon LI. Use of the zebrafish system to study primitive and definitive hematopoiesis. Annu Rev Genet 2005;39:481–501. [PubMed: 16285869]

Deniziak M, Thisse C, Rederstorff M, Hindelang C, Thisse B, Lescure A. Loss of selenoprotein N function causes disruption of muscle architecture in the zebrafish embryo. Exp Cell Res. 2006

Etard C, Behra M, Ertzer R, Fischer N, Jesuthasan S, Blader P, Geisler R, Strahle U. Mutation in the delta-subunit of the nAChR suppresses the muscle defects caused by lack of Dystrophin. Dev Dyn 2005;234:1016–1025. [PubMed: 16245342]

Felsenfeld AL, Walker C, Westerfield M, Kimmel C, Streisinger G. Mutations affecting skeletal muscle myofibril structure in the zebrafish. Development 1990;108:443–459. [PubMed: 2340809]

Formigli L, Lombardo LD, Adembri C, Brunelleschi S, Ferrari E, Novelli GP. Neutrophils as mediators of human skeletal muscle ischemia-reperfusion syndrome. Hum Pathol 1992;23:627–634. [PubMed: 1592384]

Gavrieli Y, Sherman Y, Ben-Sasson SA. Identification of programmed cell death in situ via specific labeling of nuclear DNA fragmentation. J Cell Biol 1992;119:493–501. [PubMed: 1400587]

Granato M, van Eeden FJ, Schach U, Trowe T, Brand M, Furutani-Seiki M, Haffter P, Hammerschmidt M, Heisenberg CP, Jiang YJ, Kane DA, Kelsh RN, Mullins MC, Odenthal J, Nusslein-Volhard C. Genes controlling and mediating locomotion behavior of the zebrafish embryo and larva. Development 1996;123:399–413. [PubMed: 9007258]

Grounds MD, Torrisi J. Anti-TNFalpha (Remicade) therapy protects dystrophic skeletal muscle from necrosis. Faseb J 2004;18:676–682. [PubMed: 15054089]

Guyon JR, Mosley AN, Zhou Y, O'Brien KF, Sheng X, Chiang K, Davidson AJ, Volinski JM, Zon LI, Kunkel LM. The dystrophin associated protein complex in zebrafish. Hum Mol Genet 2003;12:601–615. [PubMed: 12620966]

Hall C, Flores MV, Storm T, Crosier K, Crosier P. The zebrafish lysozyme C promoter drives myeloid-specific expression in transgenic fish. BMC Dev Biol 2007;7:42. [PubMed: 17477879]

Herbomel P, Thisse B, Thisse C. Ontogeny and behaviour of early macrophages in the zebrafish embryo. Development 1999;126:3735–3745. [PubMed: 10433904]

Herbomel P, Thisse B, Thisse C. Zebrafish early macrophages colonize cephalic mesenchyme and developing brain, retina, and epidermis through a M-CSF receptor-dependent invasive process. Dev Biol 2001;238:274–288. [PubMed: 11784010]

Hodgetts S, Radley H, Davies M, Grounds MD. Reduced necrosis of dystrophic muscle by depletion of host neutrophils, or blocking TNFalpha function with Etanercept in mdx mice. Neuromuscul Disord 2006;16:591–602. [PubMed: 16935507]

Hsu K, Traver D, Kutok JL, Hagen A, Liu TX, Paw BH, Rhodes J, Berman JN, Zon LI, Kanki JP, Look AT. The pu.1 promoter drives myeloid gene expression in zebrafish. Blood 2004;104:1291–1297. [PubMed: 14996705]

Johmura Y, Osada S, Nishizuka M, Imagawa M. FAD24 acts in concert with histone acetyltransferase HBO1 to promote adipogenesis by controlling DNA replication. J Biol Chem. 2007

Johmura Y, Suzuki M, Osada S, Nishizuka M, Imagawa M. FAD24, a regulator of adipogenesis and DNA replication, inhibits H-RAS-mediated transformation by repressing NF-kappaB activity. Biochem Biophys Res Commun. 2008

Kawakami K, Takeda H, Kawakami N, Kobayashi M, Matsuda N, Mishina M. A transposon-mediated gene trap approach identifies developmentally regulated genes in zebrafish. Dev Cell 2004;7:133–144. [PubMed: 15239961]

Kimmel CB, Ballard WW, Kimmel SR, Ullmann B, Schilling TF. Stages of embryonic development of the zebrafish. Dev Dyn 1995;203:253–310. [PubMed: 8589427]

Langheinrich U, Hennen E, Stott G, Vacun G. Zebrafish as a model organism for the identification and characterization of drugs and genes affecting p53 signaling. Curr Biol 2002;12:2023–2028. [PubMed: 12477391]

Le Guyader D, Redd MJ, Colucci-Guyon E, Murayama E, Kissa K, Briolat V, Mordelet E, Zapata A, Shinomiya H, Herbomel P. Origins and unconventional behavior of neutrophils in developing zebrafish. Blood 2008;111:132–141. [PubMed: 17875807]

Martinon F, Tschopp J. Inflammatory caspases and inflammasomes: master switches of inflammation. Cell Death Differ 2007;14:10–22. [PubMed: 16977329]

Mathias JR, Dodd ME, Walters KB, Rhodes J, Kanki JP, Look AT, Huttenlocher A. Live imaging of chronic inflammation caused by mutation of zebrafish Hai1. J Cell Sci 2007;120:3372–3383. [PubMed: 17881499]

Mathias JR, Perrin BJ, Liu TX, Kanki J, Look AT, Huttenlocher A. Resolution of inflammation by retrograde chemotaxis of neutrophils in transgenic zebrafish. J Leukoc Biol. 2006

Meijer AH, van der Sar AM, Cunha C, Lamers GE, Laplante MA, Kikuta H, Bitter W, Becker TS, Spaink HP. Identification and real-time imaging of a myc-expressing neutrophil population involved in inflammation and mycobacterial granuloma formation in zebrafish. Dev Comp Immunol. 2007

Miller JD, Neely MN. Zebrafish as a model host for streptococcal pathogenesis. Acta Trop 2004;91:53–68. [PubMed: 15158689]

Nusslein-Volhard, CaD; R. Zebrafish, A Practical Approach. New York: Oxford University Press; 2002.

Onnebo SM, Yoong SH, Ward AC. Harnessing zebrafish for the study of white blood cell development and its perturbation. Exp Hematol 2004;32:789–796. [PubMed: 15345279]

Parichy DM, Ransom DG, Paw B, Zon LI, Johnson SL. An orthologue of the kit-related gene fms is required for development of neural crest-derived xanthophores and a subpopulation of adult melanocytes in the zebrafish, Danio rerio. Development 2000;127:3031–3044. [PubMed: 10862741]

Parng C, Seng WL, Semino C, McGrath P. Zebrafish: a preclinical model for drug screening. Assay Drug Dev Technol 2002;1:41–48. [PubMed: 15090155]

Parsons MJ, Campos I, Hirst EM, Stemple DL. Removal of dystroglycan causes severe muscular dystrophy in zebrafish embryos. Development 2002;129:3505–3512. [PubMed: 12091319]

Raldua D, Andre M, Babin PJ. Clofibrate and gemfibrozil induce an embryonic malabsorption syndrome in zebrafish. Toxicol Appl Pharmacol 2008;228:301–314. [PubMed: 18358510]

Renshaw SA, Loynes CA, Trushell DM, Elworthy S, Ingham PW, Whyte MK. A transgenic zebrafish model of neutrophilic inflammation. Blood. 2006

Rhodes J, Hagen A, Hsu K, Deng M, Liu TX, Look AT, Kanki JP. Interplay of pu.1 and gata1 determines myelo-erythroid progenitor cell fate in zebrafish. Dev Cell 2005;8:97–108. [PubMed: 15621533]

Schlegel A, Stainier DY. Microsomal Triglyceride Transfer Protein Is Required for Yolk Lipid Utilization and Absorption of Dietary Lipids in Zebrafish Larvae. Biochemistry 2006;45:15179–15187. [PubMed: 17176039]

Schlombs K, Wagner T, Scheel J. Site-1 protease is required for cartilage development in zebrafish. Proc Natl Acad Sci U S A 2003;100:14024–14029. [PubMed: 14612568]

Seeley M, Huang W, Chen Z, Wolff WO, Lin X, Xu X. Depletion of zebrafish titin reduces cardiac contractility by disrupting the assembly of Z-discs and A-bands. Circ Res 2007;100:238–245. [PubMed: 17170364]

Steffen LS, Guyon JR, Vogel ED, Howell MH, Zhou Y, Weber GJ, Zon LI, Kunkel LM. The zebrafish runzel muscular dystrophy is linked to the titin gene. Dev Biol 2007;309:180–192. [PubMed: 17678642]

Su F, Juarez MA, Cooke CL, Lapointe L, Shavit JA, Yamaoka JS, Lyons SE. Differential Regulation of Primitive Myelopoiesis in the Zebrafish by Spi-1/Pu.1 and C/ebp1. Zebrafish 2007;4:187–199. [PubMed: 18041923]

Thisse B, Heyer V, Lux A, Alunni V, Degrave A, Seiliez I, Kirchner J, Parkhill JP, Thisse C. Spatial and temporal expression of the zebrafish genome by large-scale in situ hybridization screening. Methods Cell Biol 2004;77:505–519. [PubMed: 15602929]

Thisse, B.; Pflumio, S.; Fürthauer, M.; Loppin, B.; Heyer, V.; Degrave, A.; Woehl, R.; Lux, A.; Steffan, T.; Charbonnier, XQ.; Thisse, C. Expression of the zebrafish genome during embryogenesis. 2001. ZFIN Direct Data Submission (Unpublished) http://zfin.org/cgi-bin/webdriver?MIval=aa-pubview2.apg&OID=ZDB-PUB-010810-1

Thornberry NA, Bull HG, Calaycay JR, Chapman KT, Howard AD, Kostura MJ, Miller DK, Molineaux SM, Weidner JR, Aunins J, et al. A novel heterodimeric cysteine protease is required for interleukin-1 beta processing in monocytes. Nature 1992;356:768–774. [PubMed: 1574116]

Tominaga K, Johmura Y, Nishizuka M, Imagawa M. Fad24, a mammalian homolog of Noc3p, is a positive regulator in adipocyte differentiation. J Cell Sci 2004;117:6217–6226. [PubMed: 15564382]

Tucker B, Lardelli M. A rapid apoptosis assay measuring relative acridine orange fluorescence in zebrafish embryos. Zebrafish 2007;4:113–116. [PubMed: 18041929]

Urasaki A, Morvan G, Kawakami K. Functional dissection of the Tol2 transposable element identified the minimal cis-sequence and a highly repetitive sequence in the subterminal region essential for transposition. Genetics 2006;174:639–649. [PubMed: 16959904]

van der Sar AM, Musters RJ, van Eeden FJ, Appelmelk BJ, Vandenbroucke-Grauls CM, Bitter W. Zebrafish embryos as a model host for the real time analysis of Salmonella typhimurium infections. Cell Microbiol 2003;5:601–611. [PubMed: 12925130]

Whitehead NP, Yeung EW, Allen DG. Muscle damage in mdx (dystrophic) mice: role of calcium and reactive oxygen species. Clin Exp Pharmacol Physiol 2006;33:657–662. [PubMed: 16789936]

Wisse BE. The inflammatory syndrome: the role of adipose tissue cytokines in metabolic disorders linked to obesity. J Am Soc Nephrol 2004;15:2792–2800. [PubMed: 15504932]

Xu X, Meiler SE, Zhong TP, Mohideen M, Crossley DA, Burggren WW, Fishman MC. Cardiomyopathy in zebrafish due to mutation in an alternatively spliced exon of titin. Nat Genet 2002;30:205–209. [PubMed: 11788825]

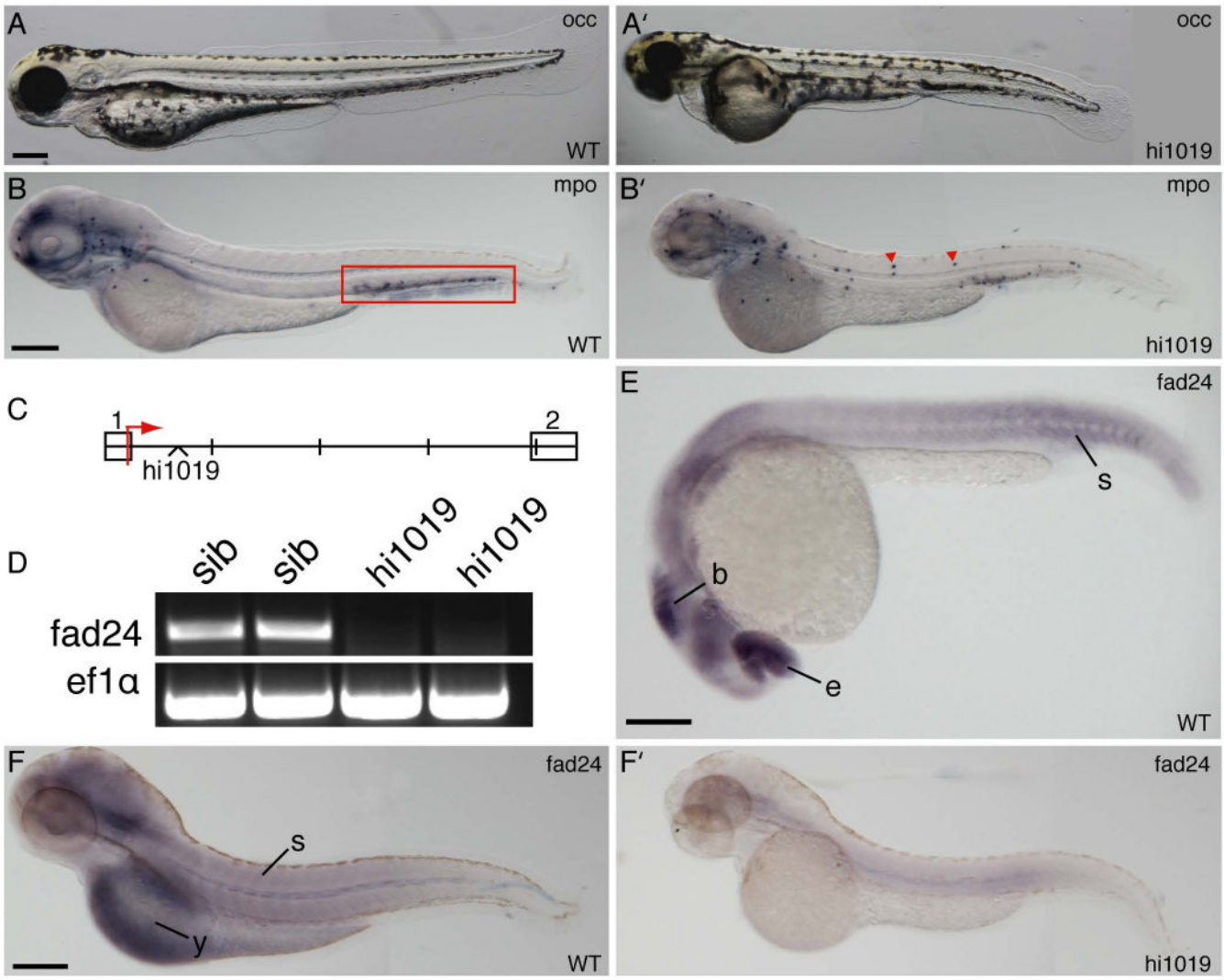

Figure 1. Fad24^{hi1019} mutants exhibit a chronic inflammatory phenotype and reduced expression of *fad24*

(A,A′) Oblique coherent contrast (OCC) images of WT and homozygous fad24^{hi1019} larvae at 3 dpf. (B,B′) Zebrafish *mpo* in situ hybridizations of WT and fad24^{hi1019} larvae at 3 dpf, box indicates the CHT and arrows indicate neutrophils in the body of fad24^{hi1019} mutants. (C) Genomic map of the first two exons of zebrafish *fad24* showing the location of the *hi1019* insertion, each section = 500 bp. (D) RT-PCR analysis of WT (lanes 1,2) and fad24^{hi1019} mutant (lanes 3,4) single larvae at 3 dpf, *ef1α* is used as a control. (E, F, F′) In situ hybridization of zebrafish *fad24* in WT (E,F) and fad24^{hi1019} mutants (F′) at 26 hpf (E) and 3 dpf (F,F′), b = brain, e = eye, s = somite and y = yolk. Lateral view, anterior to the left. Bars = 200 μm. Representative results from at least three experiments with greater than 10 larvae per condition per experiment.

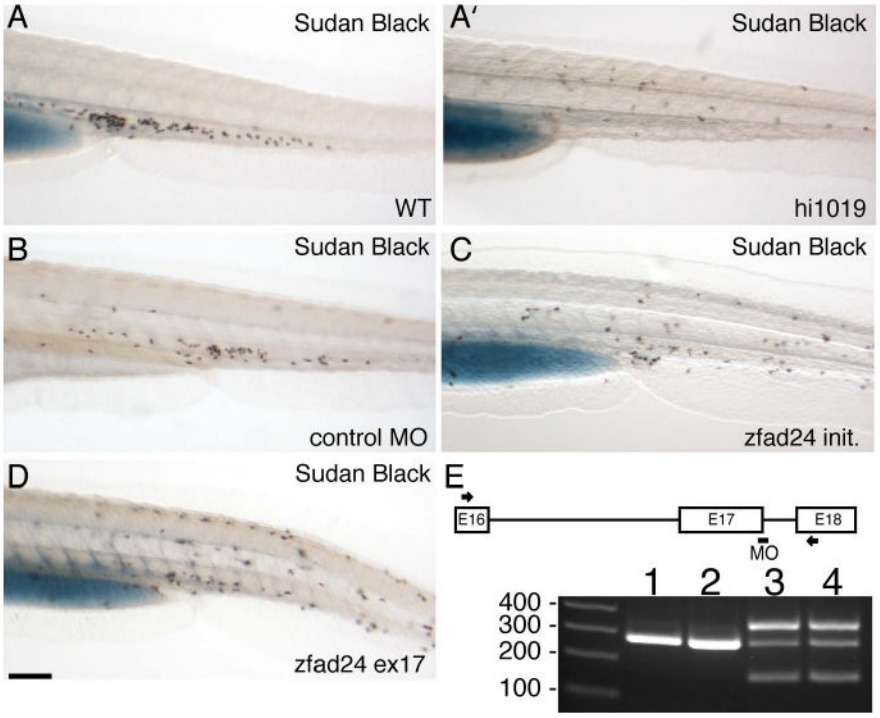

F

			Neutrophil Location			
	MO injected	n	CHT	Body	Total	% in Body
WT	-	17	40.1±2.4	5.1±1.3	45.2±3.2	9.9
hi1019	-	21	9.1±1.1	19.8±2.6	29.0±3.2	67.7*
WT	standard con.	15	46.0±3.0	11.3±2.1	57.3±3.9	18.9
WT	zfad24 init.	21	22.5±1.7	20.5±1.8	43.0±2.6	47.0*
WT	zfad24 ex. 17	21	25.4±2.5	21.5±1.7	46.4±3.2	47.4*

Figure 2. Injection of *fad24* MO into WT embryos phenocopies the fad24^{hi1019} leukocyte infiltration phenotype

Shown is the CHT and surrounding tissues of sudan black stained WT (A) and fad24^{hi1019} (A ′) larvae or control MO (B), zfad24 init. MO (C), or zfad24 ex17 MO (D) injected larvae. Lateral view, anterior to the left at 3 dpf. Bar = 200 μm. (E) Schematic *of fad24* exon 16, 17 and 18 with the target site of the zfad24 ex17 MO labeled, arrows indicate locations of primers used for RT-PCR of total RNA isolated from single embryos at 24 hours post injection of either uninjected (lane 1), standard control (lane 2) or zfad24 ex17 (lane 3 and 4) MO. (F) Quantification of neutrophil location (either in the CHT or in the body) seen in WT and fad24^{hi1019} larvae or control MO, zfad24 init. MO, or ex17 MO injected larvae analyzed by one-way ANOVA at a 95% confidence level using Dunnett's multiple comparison post test, * = p-value <.05. Results reported as average ± SEM.

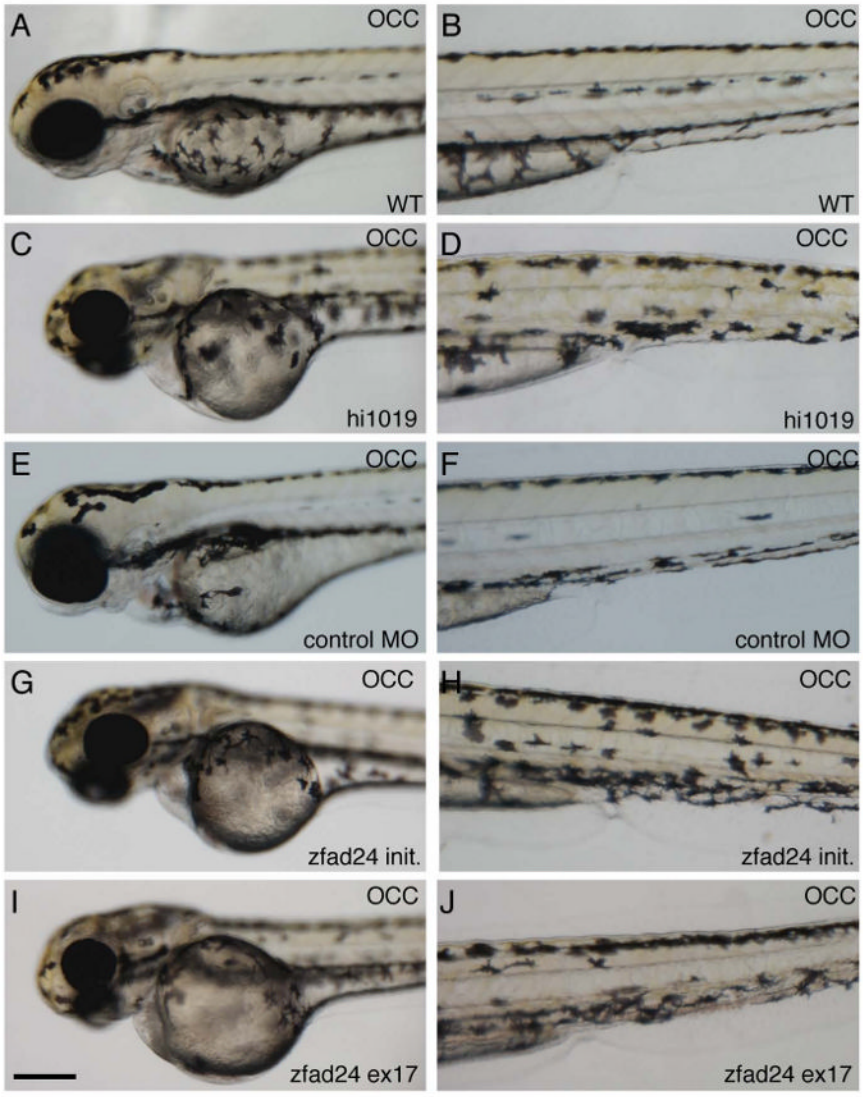

K

	Length of yolk (μm)	Length of eye (μm)
WT	405.5 ± 12.5	239.7 ± 3.4
hi1019	484.2 ± 6.0*	211.0 ± 2.7*
control MO	409.9 ± 10.5	248.0 ± 2.8
zfad24 init	492.6 ± 12.6*	216.4 ± 2.4*
zfad24 ex. 17	516.1 ± 11.8*	209.8 ± 4.9*

Figure 3. Injection of *fad24* MOs into WT embryos phenocopies the fad24^{hi1019} morphological phenotypes

OCC images of the head and yolk (A,C,E,G,I) or body (B,D,F,H,J) of WT (A,B) and fad24^{hi1019} (C,D) larvae or control MO (E,F), zfad24 init. MO (G,H), or zfad24 ex17 MO (I,J) injected larvae. (K) Comparison of yolk sac and eye length for WT and fad24^{hi1019} larvae or control MO, zfad24 init. MO, or zfad24 ex17 MO injected larvae. Results reported as average ± SEM, analyzed by one-way ANOVA at a 95% confidence level using Dunnett's multiple comparison post test, * = p-value <.05. Representative results from three experiments.

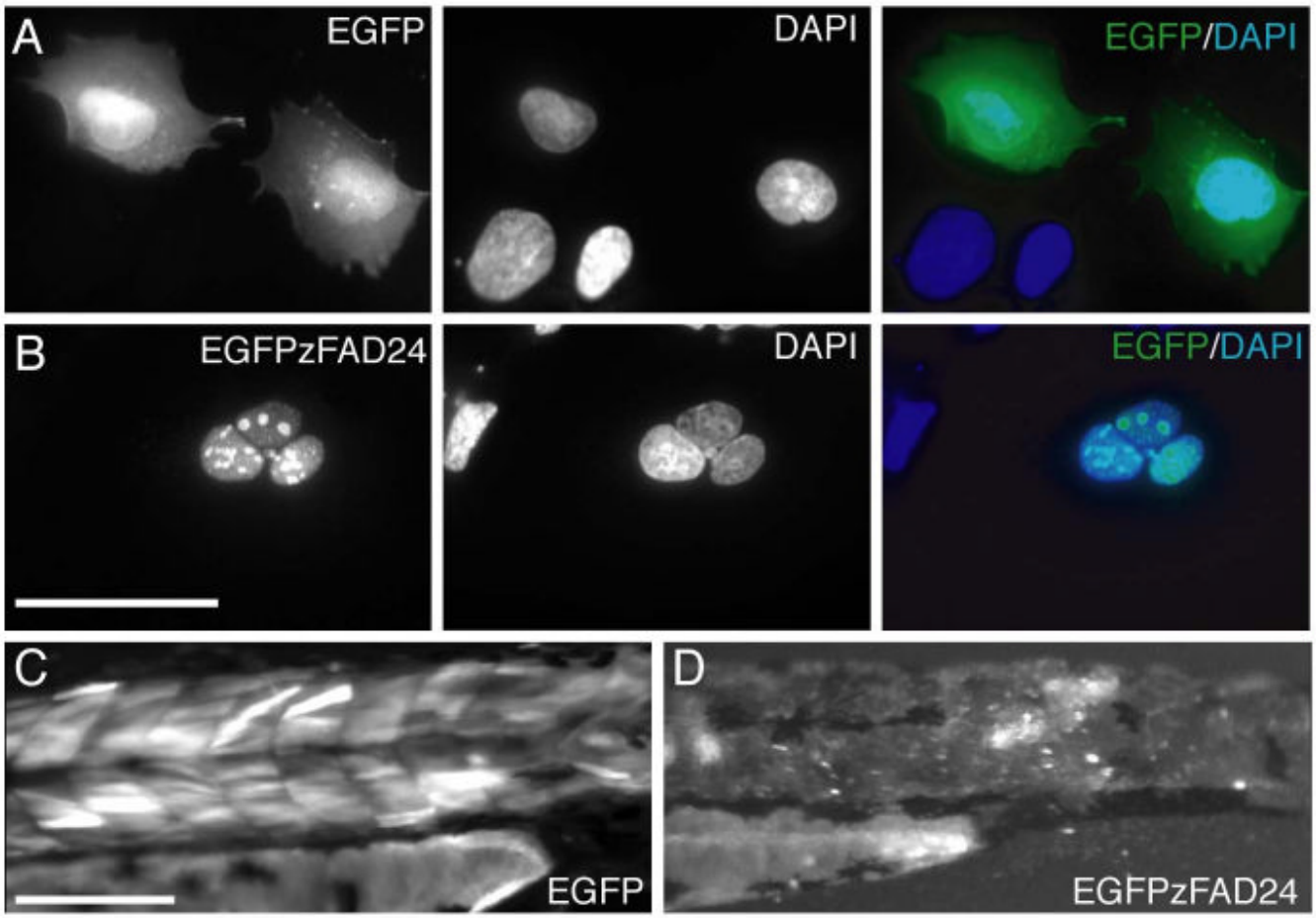

Figure 4. Zebrafish fad24 localizes to nuclear granules

HEK cells transfected with EGFP (A) or N-terminal EGFP tagged zebrafish Fad24 (B). DAPI staining is used to reveal the nucleus, Bar = 50 μm. Transient expression of EGFP (C) or N-terminal EGFP tagged zebrafish Fad24 (D) in muscle cells of 3 dpf WT larvae. Representative results from three experiments.

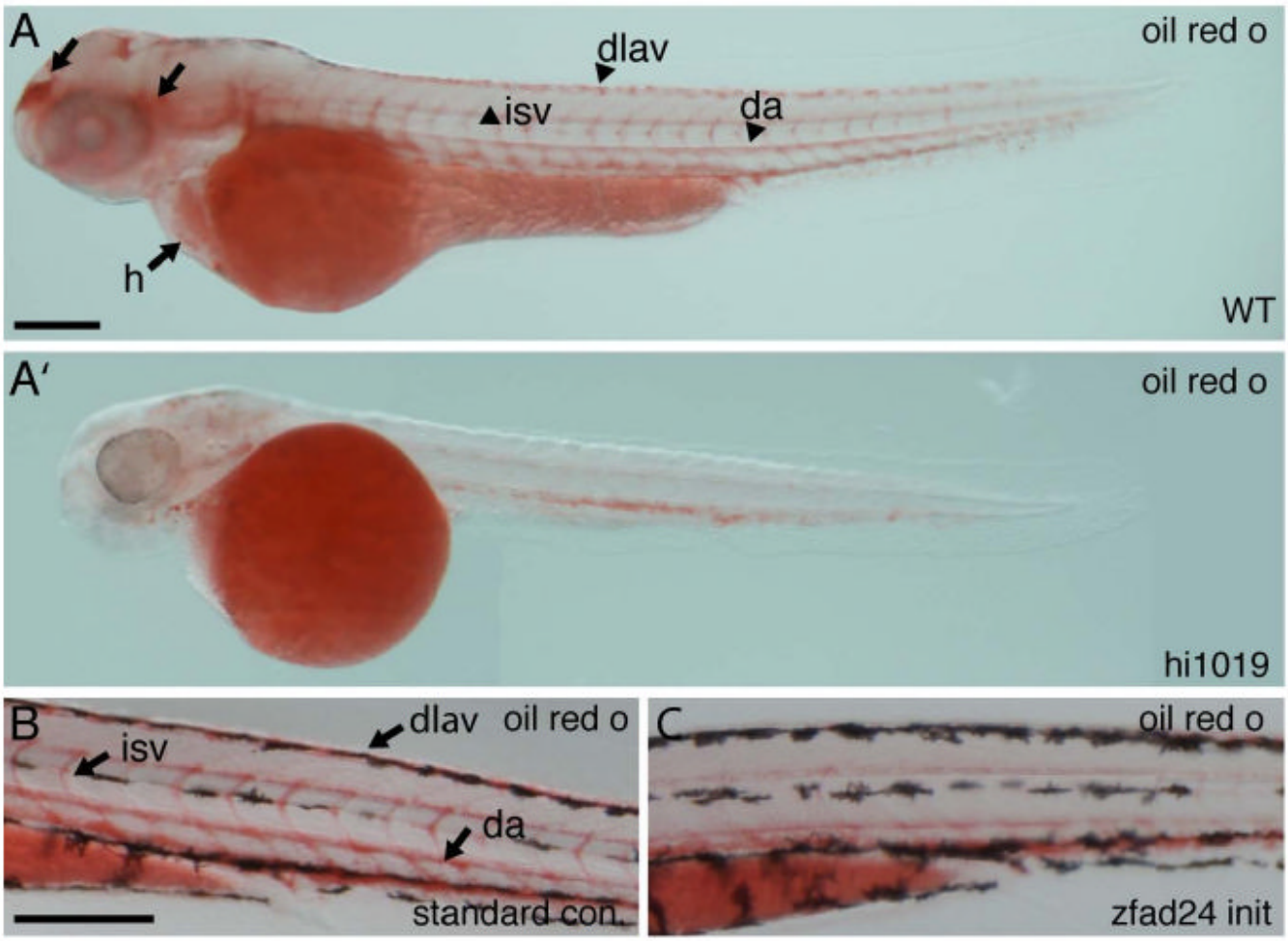

Figure 5. Fad24^{hi1019} mutants exhibit defects in lipid metabolism

(A, A′) Oil red O staining in a PTU treated WT (A) and fad24^{hi1019} (A′) larvae, arrows show areas of staining in the head and heart, and arrowheads show areas of staining in the vasculature that are absent in the fad24^{hi1019} mutant. (B, C) Oil red O staining in the body of control (B) or zfad24 init. MO (C) injected larvae. h = heart, isv = intersegmental vessel, da = dorsal aorta and dlav = dorsal longitudinal anastomotic vessel. Lateral view, anterior to the left at 3 dpf. Bars = 200 μm. Representative results from three experiments with greater than 10 larvae per condition per experiment.

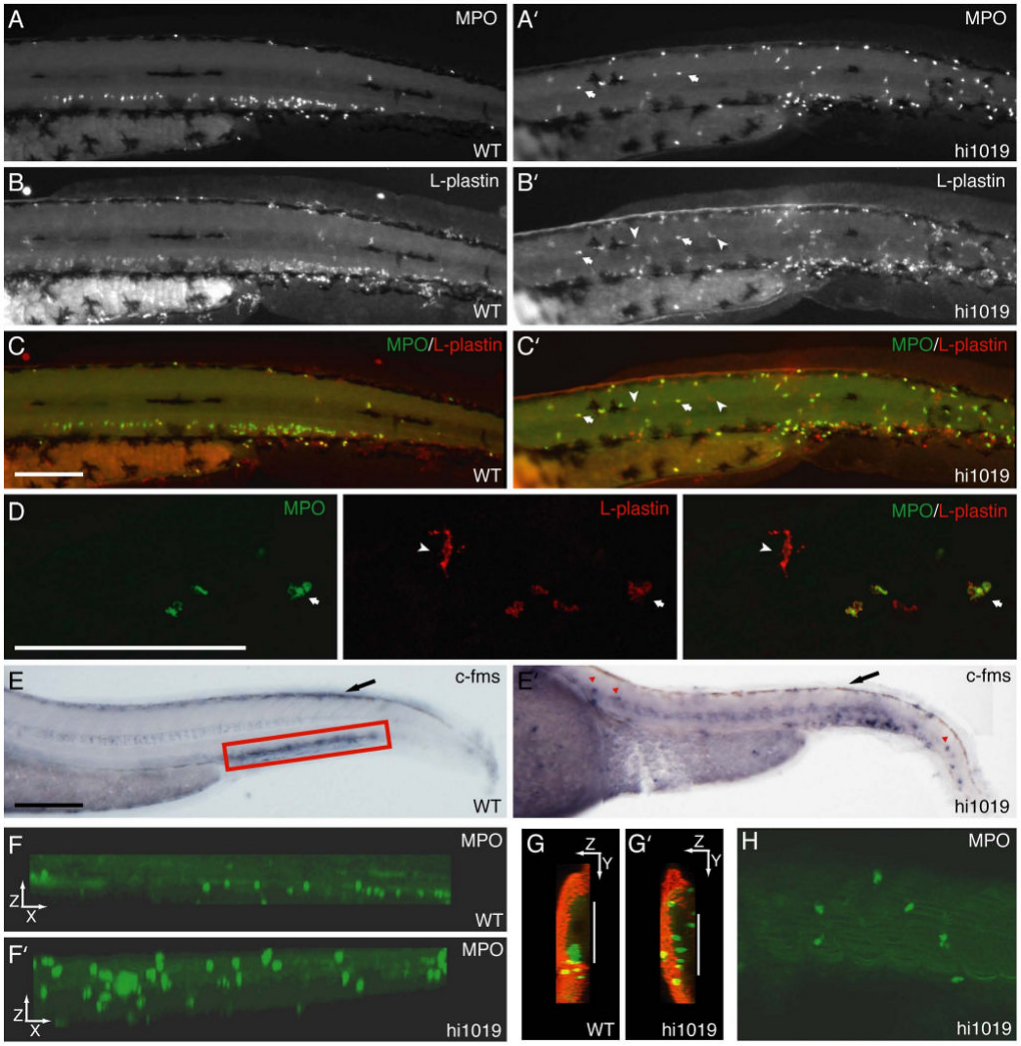

Figure 6. Leukocyte recruitment into the body of fad24^{hi1019} mutants

A-C are WT and A′-C′ are fad24^{hi1019} mutant larvae. Immunolabeling for MPO (A,A′) and L-plastin (B,B′). (C,C′) Overlay of MPO and L-plastin co-immunolabeling shows that neutrophils, MPO^{+} and L-plastin^{+} (arrows), and macrophages, L-plastin^{+} and MPO^{-} cells (arrowhead), contribute to the inflammatory response. (D) Confocal projections show the more elongated morphology of macrophages (arrowhead) compared to neutrophils (arrow). (E,E′) Whole-mount in situ hybridization for *c-fms*, a macrophage marker, red box indicates the CHT, and red arrows indicate macrophages in the body of fad24^{hi1019} mutants. Black arrows point to *c-fms* expression in the neural crest. (F,F′) XZ projections of MPO labeled WT and fad24^{hi1019} larvae. (G,G′) ZY projections of MPO (green) and p63 (red, to mark the epidermis) double-immunolabeled larvae, white line indicates the midline of the larva. (H) A 3.9 μm optical longitudinal section through the muscle of a fad24^{hi1019} larvae immunolabeled for MPO. All images except F,F′G,G′ are in lateral view, anterior to the left and all images are at 3 dpf. Bars = 200 μm. Representative results from three experiments.

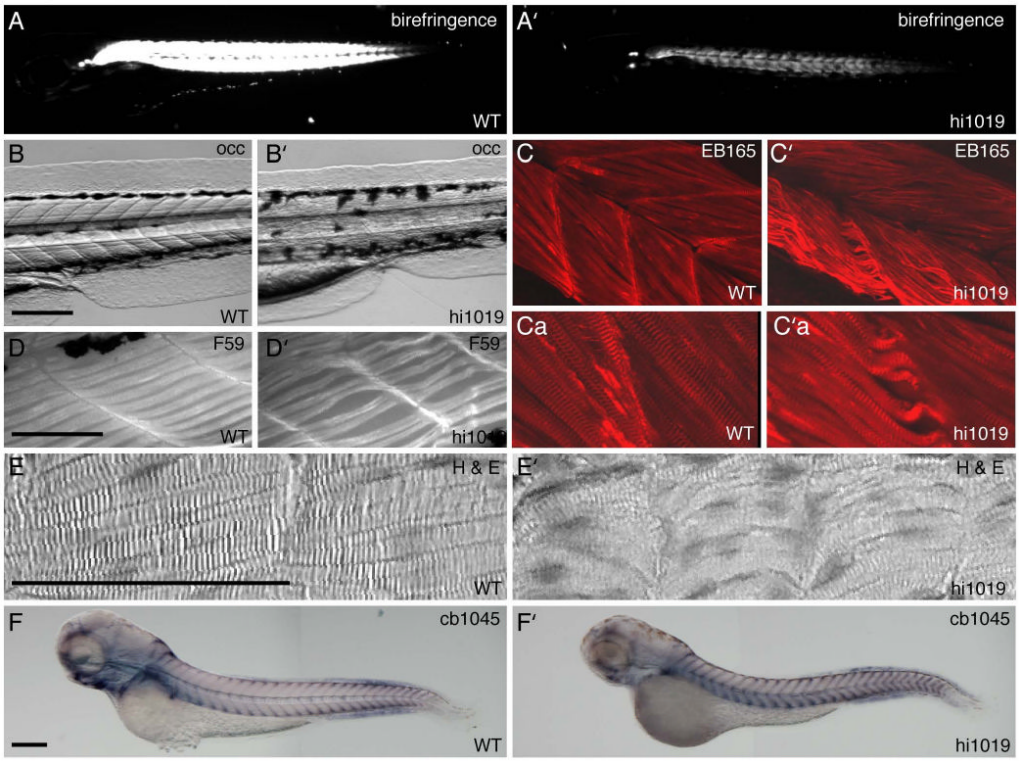

Figure 7. Fad24^{hi1019} mutants exhibit muscle degeneration

A-F are WT and A′-F′ are fad24^{hi1019} mutant larvae. (A,A′) Polarized light microscopy to reveal birefringence of muscle. (B,B′) OCC images of trunk muscle. (C,C′) Confocal projections of trunk muscle immunolabeled with the fast-muscle myosin specific antibody EB165. (Ca,C′a) Zoomed in images better showing muscle fiber striation and size. (D,D′) Immunolabeling with the slow-muscle myosin specific antibody F59. (E,E′) Hematoxylin and Eosin-stained lateral sections through trunk muscle tissue. (F,F′) In situ hybridization using probe cb1045 to reveal myoseptum separating the somites of developing larvae. Lateral view, anterior to the left at 3 dpf. Bars = 200 μm. Representative results from three experiments with greater than 10 larvae per condition per experiment.

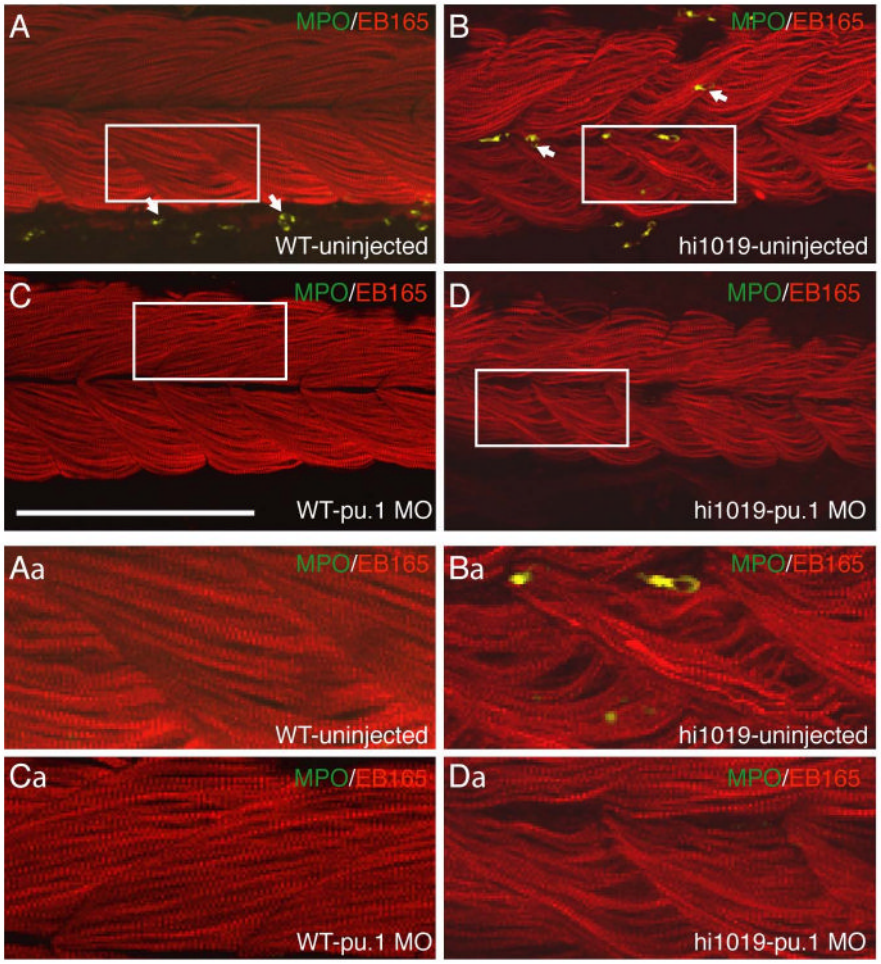

Figure 8. Onset of muscle degeneration in fad24^{hi1019} mutants is not mediated by leukocytes

Tailfin views at 3 dpf. A,C are WT, B,D are fad24^{hi1019} mutants. (A,B,C,D) Co-immunolabeling for zMPO (green) and fast-muscle myosin (red) in uninjected (A,B) and *pu.1* MO injected (C,D) larvae, arrows indicated neutrophils. White boxes indicated areas magnified in Aa,Ba,Ca,Da. Lateral view with anterior to the left. Bar = 200 μm. Representative results from three experiments.

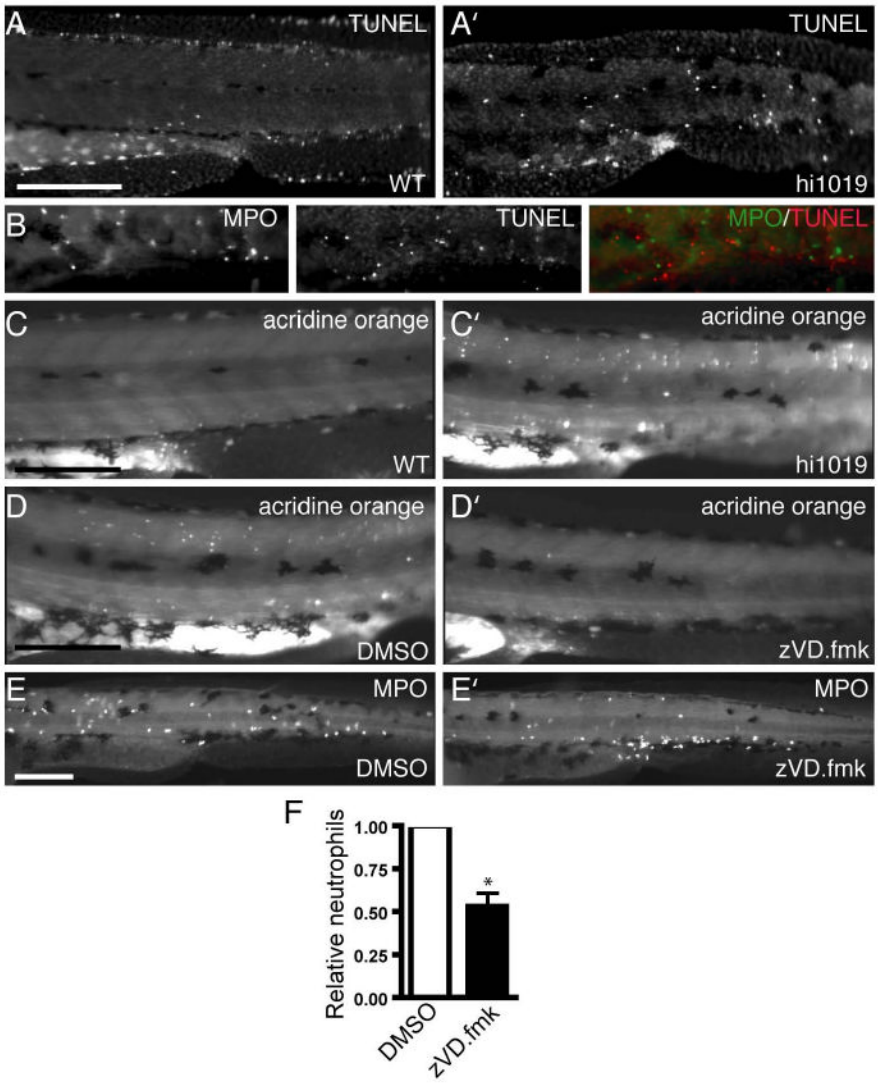

Figure 9. Apoptosis is partially responsible for the recruitment of neutrophils to the trunk of fad24^{hi1019} mutant larvae

(A,A′) TUNEL staining in the trunk of WT (A) and fad24^{hi1019} mutants (A′). (B) TUNEL staining in fad24^{hi1019} mutant coimmunolabeled with MPO. (C,C′) Acridine orange staining in the trunk of WT (C) and fad24^{hi1019} mutant (C′) larvae. (D,D′) Acridine orange staining in fad24^{hi1019} larvae can be blocked by the addition of the pan-caspase inhibitor zVD.fmk (D′) to the larvae water but not by addition of the vehicle control, DMSO (D). (E,E′) MPO immunolabeling of DMSO (E) and zVD.fmk (E′) treated fad24^{hi1019} larvae. (F) Quantification of neutrophils found in the body of fad24^{hi1019} larvae when treated with zVD.fmk relative to the vehicle control, DMSO (set to 100%). Average of three replicates analyzed by a paired student's t-test at a 95% confidence level, * = p-value <.05, error bar is standard error of the mean. Lateral view with anterior to the left at 3 dpf. Bars except C = 200 μm. Representative results from three experiments with greater than 10 larvae per condition per experiment.